Available online at www.sciencedirect.com
ScienceDirect
Solid-State Electronics 52 (2008) 11–16
SOLID-STATE ELECTRONICS
www.elsevier.com/locate/sse

Studying the effect of material parameters on detectivity in a p–n $In_{0.53}Ga_{0.47}As$ photovoltaic detector

Longhai Li [a], Jingzhi Yin [a,*], Bao Shi [a], Minshuai Wang [a], Guotong Du [a], Yiding Wang [a], Yixin Jin [b]

[a] *State Key Laboratory on Integrated Optoelectronics, College of Electronic Science and Engineering, Jilin University, 2699 Qianjin Street, Changchun 130012, Peoples Republic of China*

[b] *Changchun Institute of Optics, Fine Mechanics and Physics, Chinese Academy of Sciences, Changchun 130033, People's Republic of China*

Received 6 September 2006; received in revised form 14 June 2007; accepted 25 July 2007
Available online 10 September 2007

The review of this paper was arranged by Prof. Y. Arakawa

Abstract

In the paper, a relationship of detectivity with material parameters is given by a theoretical calculation. An $In_{1-x}Ga_xAs$ photovoltaic detector structure with $x = 0.47$ is used as an example for this study. The results show that the detectivity of a photodetector can be enhanced by optimizing the carrier concentration, thickness and surface recombination velocity during the structure growth and device fabrication.
© 2007 Elsevier Ltd. All rights reserved.

1. Introduction

Indium gallium arsenide (InGaAs) is an alloy of indium arsenide and gallium arsenide. The bandgap of the $In_{1-x}Ga_xAs$ ternary system changes from $E_{g\ InAs} = 0.35$ eV (3.5 μm) to $E_{g\ GaAs} = 1.43$ eV (0.87 μm). $In_{0.53}Ga_{0.47}As$ alloy ($E_g = 0.73$ eV, $\lambda_c = 1.7$ μm) lattice matched to the InP substrate has already been shown to be a suitable photodetector material for near-IR (1.0–1.7 μm) applications [1]. Comparing with indirect-bandgap germanium photodetector, the InGaAs photodetector is superior to its lower dark current and low noise figure. Such a photodetector has many commercial and military applications, such as remote light communication systems, low light level night vision, remote sensing, eye-safe range finding and process control [2–8]. One of the important figures of merit of the photovoltaic detectors is its detectivity. The detectivity is mainly defined by the zero-bias resistance area product (R_0A) and quantum efficiency. In the paper, we dissect the dependence of R_0A and quantum efficiency on material parameters for a p–n $In_{0.53}Ga_{0.47}As$ photovoltaic detector. A relationship of detectivity with material parameters is given by the R_0A and quantum efficiency.

2. Theoretical analysis

A photovoltaic detector is built by a homogenous n-p junction of InGaAs lattice-matched to the InP substrate. Shown in Fig. 1 is a schematic of such a photodetector structure. S_e and S_p is the surface recombination velocity of the electron and hole, respectively.

The basic expression of the detector D^* is given by [9]

$$D^* = \frac{\eta q}{h\nu}\sqrt{\frac{R_0A}{4kT}}, \tag{1}$$

where R_0A is the product of resistance at zero bias voltage and detecting area, the k is the Boltzmann constant, T is the work temperature, $h\nu$ is the energy of the incident light, η is quantum efficiency, q is the electron charge and c is the velocity of light.

* Corresponding author.
E-mail address: yjz886666@yahoo.com.cn (J. Yin).

0038-1101/$ - see front matter © 2007 Elsevier Ltd. All rights reserved.
doi:10.1016/j.sse.2007.07.032

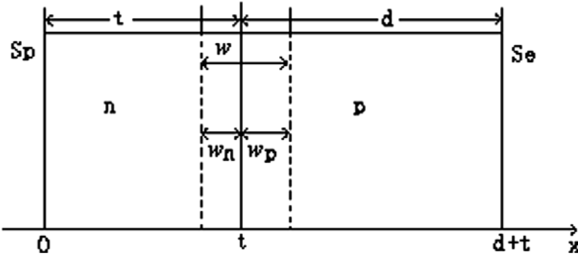

Fig. 1. The simple structure of InGaAs detector.

When the energy of the incident light is larger than the bandgap of material, the absorbing occurs. The maximum wavelength of the incident light is gotten by $\lambda = \lambda_c = hc/E_g$ (E_g is the bandgap of the material). Eq. (1) can be simplified to the following:

$$D^* = \frac{q\eta}{E_g}\sqrt{\frac{R_0A}{4kT}}. \tag{2}$$

When temperature and material composition are selected, the bandgap E_g is fixed. From Eq. (2), we know that D^* is determined only by R_0A and η.

2.1. R_0A of the various kinds of noise mechanisms

R_0A is related to various kinds of noise mechanisms. Because all the noise mechanisms are independent, $(R_0A)_{\text{Total}}$ may be expressed by [10]

$$\frac{1}{(R_0A)_{\text{Total}}} = \frac{1}{(R_0A)_{\text{Auger}}} + \frac{1}{(R_0A)_{\text{Rad}}} + \frac{1}{(R_0A)_{\text{GR}}} + \frac{1}{(R_0A)_{\text{Tunnel}}}, \tag{3}$$

where $(R_0A)_{\text{Auger}}$, $(R_0A)_{\text{Rad}}$, $(R_0A)_{\text{GR}}$, and $(R_0A)_{\text{Tunnel}}$ denote the Auger, radiation, G–R and tunnel mechanism, respectively.

For the Auger and radiative mechanism, $(R_0A)_{\text{Auger}}$, $(R_0A)_{\text{Rad}}$ are expressed as follows [10]:

$$(R_0A)_j = \frac{kT}{q^2}\left[\frac{D_p n_i^2}{L_p n}\frac{r_p ch(\frac{t-w_n}{L_p}) + sh(\frac{t-w_n}{L_p})}{r_p sh(\frac{t-w_n}{L_p}) + ch(\frac{t-w_n}{L_p})} + \frac{D_e n_i^2}{L_e p}\frac{r_e ch(\frac{d-w_p}{L_e}) + sh(\frac{d-w_p}{L_e})}{r_e sh(\frac{d-w_p}{L_e}) + ch(\frac{d-w_p}{L_e})}\right]^{-1}, \tag{4}$$

where $r_i = L_iS_i/D_i$ and $D_i = kT\mu_i/q$; D_i is the diffusion coefficient (cm^2/s) for holes in the n-region or for electrons in the p-region; μ_i, effective mobility (cm^2 V^{-1} s^{-1}) for holes or electrons; S_i, surface recombination velocity (m/s) for holes in the n-region or for electrons in the p-region; $L_i = (D_i\tau_i)^{1/2}$, diffusion length (cm) for holes in the n-region or for electrons in the p-region; t, d, the thickness (cm) for the n-region and p-region, respectively, w_n, w_p, depletion region thickness (cm) for the n-region and p-region, respectively; p, n, carrier concentration for the p-region and n-region, respectively; n_i is the intrinsic carrier concentration.

From Eq. (4), it is found that $(R_0A)_j$ is affected by either minority lifetimes of the Auger mechanism $(R_0A)_{\text{Auger}}$ or the radiative mechanism $(R_0A)_{\text{Rad}}$. The expression of Auger lifetime is given in [9] and the radiative lifetime can be obtained by [10]

$$\tau_R^h = \frac{1}{B[n + (n_i^2/n)]} \quad \text{(in the n-region)}, \tag{5a}$$

$$\tau_R^e = \frac{1}{B[p + (n_i^2/p)]} \quad \text{(in the p-region)}, \tag{5b}$$

where τ_R^h, τ_R^e are the radiative lifetimes for holes in the n-region and for electrons in the p-region. B is a constant defined by

$$B = 5.8\times10^{-13}\varepsilon_\infty^{1/2}\left(\frac{1}{m_e^* + m_h^*}\right)^{3/2}\left(1 + \frac{1}{m_e^*} + \frac{1}{m_h^*}\right)\times(300/T)^{3/2}E_g^2, \tag{5c}$$

where $\varepsilon_\infty = 14$, the high-frequency dielectric constant, and m_e^*, m_h^* are the electron or hole effective mass, E_g is the InGaAs bandgap energy.

The G–R (generation–recombination) mechanism appears in the space–charge region, which is caused by lattice defects and impurities in the forbidden gap of a semiconductor material. The R_0A product associated with intrinsic carrier concentration and parameters in the depletion region is indicated to [10]:

$$(R_0A)_{\text{GR}} = \frac{\sqrt{\tau_{n0}\tau_{p0}}V_{\text{bi}}}{qn_iWf(b)}, \tag{6}$$

where τ_{n0}, τ_{p0} are the electron and hole lifetime within the depletion region, W is the width of the depletion region and V_{bi} is the built-in voltage through the p–n junction. The function $f(b)$ is a definite integral depending on the position of recombination centers in the energy gap. For simplicity, we further assume $f(b) = 1$, and $\tau_{n0} = \tau_{p0} = \tau_0 = 1/V_{\text{th}}\sigma N_f$ [11], $(R_0A)_{\text{GR}}$ is shown as following [10]

$$(R_0A)_{\text{GR}} = \frac{V_{\text{bi}}}{qn_iwV_{\text{th}}\sigma N_f}, \tag{7}$$

where $V_{\text{th}} = (3kT/m^*)^{1/2}$, σ is the capture cross section and N_f is the trap density.

In general, there are two kinds of tunneling current in the photovoltaic detector. They are direct and indirect tunneling current cross the junction [10]. Because the probability for indirect tunneling is much lower than that for direct tunneling, direct tunneling is only considered in InGaAs detectors. The R_0A with the tunneling is defined by [11]

$$(R_0A)_{\text{Tunnel}} = \frac{kT}{CT_tq(\delta_n + \delta_p)^2}, \tag{8}$$

where $C = qm^*/8\pi^2\hbar^3$ is a constant. The δ_n or δ_p is the difference between Fermi levels and conduction base or valence top (see Fig. 2). T_t is the tunneling probability determined by the potential barrier shape. Two types of potential barriers, namely triangular and parabolic barriers,

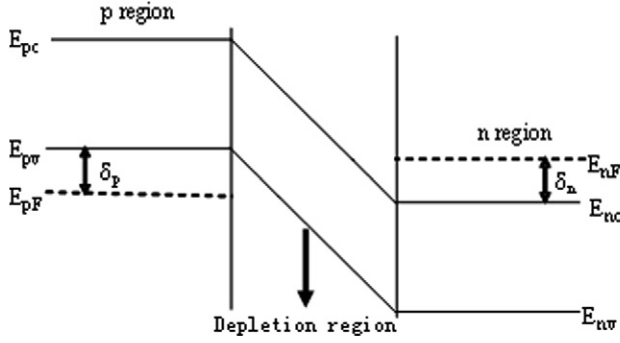

Fig. 2. The bandgap of p–n homojunction structure.

are often considered. For a triangular barrier, the probability is given by [10]

$$T_{t1} = \exp\left(-\frac{4\sqrt{2m^*}E_g^{3/2}}{3q\hbar\varepsilon}\right) \tag{9}$$

and for a parabolic barrier:

$$T_{t2} = \exp\left(-\frac{\pi\sqrt{m^*}E_g^{3/2}}{2\sqrt{2}q\hbar\varepsilon}\right), \tag{10}$$

where $\varepsilon = V_{bi}/W$ is the built-in field through the depletion region.

2.2. Quantum efficiency

The formula of the quantum efficiency within the different regions is obtained by two current density, two continuity and Poisson's equations under the condition of having light injected. When the incident light is injected from the n-region, the quantum efficiency of the n-region, p-region and depletion region is given as follows [10]:

$$\eta_n = \frac{\alpha L_h(1-r)}{(\alpha^2 L_h^2 - 1)} \times \left\{ \frac{(r_h + \alpha L_h) - e^{-\alpha(t-w_n)}\left[r_h ch\left(\frac{t-w_n}{L_h}\right) + sh\left(\frac{t-w_n}{L_h}\right)\right]}{r_h sh\left(\frac{t-w_n}{L_h}\right) + ch\left(\frac{t-w_n}{L_h}\right)} - \alpha L_h e^{-\alpha(t-w_n)} \right\}, \tag{11}$$

$$\eta_p = \frac{\alpha L_e(1-r)}{(\alpha^2 L_e^2 - 1)} e^{-\alpha(t+w_p)} \times \left\{ \alpha L_e + \frac{(r_e - \alpha L_e)e^{-\alpha(d-w_p)} - \left[r_e ch\left(\frac{d-w_p}{L_e}\right) + sh\left(\frac{d-w_p}{L_e}\right)\right]}{r_e sh\left(\frac{d-w_p}{L_e}\right) + ch\left(\frac{d-w_p}{L_e}\right)} \right\}, \tag{12}$$

$$\eta_{dr} = (1-r)[e^{-\alpha(t-w_n)} - e^{-\alpha(t+w_p)}]. \tag{13}$$

Therefore, total quantum efficiency is

$$\eta = \eta_n + \eta_p + \eta_{dr}, \tag{14}$$

where α: absorption coefficient; r: reflection coefficient.

If light is injected from the p-region, the quantum efficiency of the n-region, p-region, and depletion region is the same as (11)–(13), but corresponding parameter should be exchanged, that is $n \to p$, $r_e \to r_h$, $L_e \to L_h$, $w_p \to w_n$, $t \to d$, $p \to n$, $r_h \to r_e$, $L_h \to L_e$, $w_n \to w_p$, $d \to t$.

3. Calculation results and discussions

By the Eqs. (3)–(8), $(R_0A)_{Auger}$, $(R_0A)_{Rad}$, $(R_0A)_{GR}$, and $(R_0A)_{Tunnel}$ are obtained at 300 K. Fig. 3 shows the $(R_0A)_{total}$ and the (R_0A) components that vary with the carrier concentration of p-region, where the parameters are $d = 5$ μm, $S_e = 0$, $n = 10^{18}$ cm^{-3}, $t = 5$ μm, $S_p = 0$, $\sigma N_f = 0.1$ cm^{-1}. Moreover, mobility for holes or electrons is considered as a constant. They are $\mu_h = 400$ cm^2/V s and $\mu_e = 3000$ cm^2/V s. In fact, mobility of holes or electrons varies with carrier concentration. Our results indicate that the change is small, and only occurs in the lower (<10^{17} cm^{-3}) or higher concentration (>10^{19} cm^{-3}) (it will be reported in the other paper).

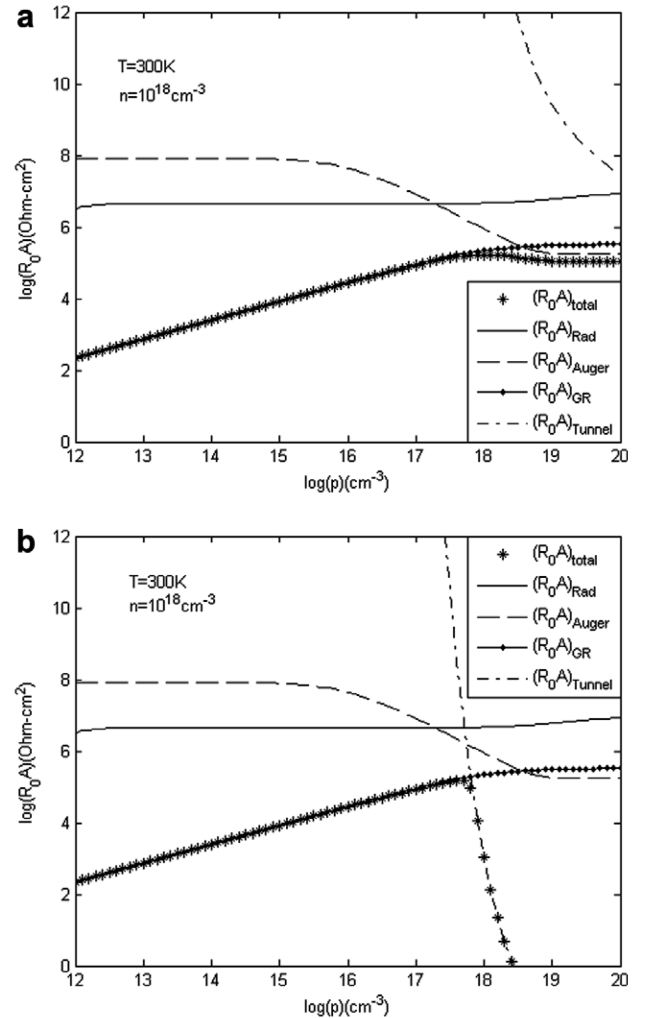

Fig. 3. The dependence of the R_0A components and total R_0A on p-side carrier concentration, (a) and (b) for the triangular barrier and the parabolic barrier, respectively. In the condition of $d = 5$ μm, $t = 5$ μm, $\mu_h = 400$ cm^2/V s, $\mu_e = 3000$ cm^2/V s, $S_p = 0$, $S_e = 0$, $\sigma N_f = 0.1$ cm^{-1}.

The situations of the triangular barrier and the parabolic barrier are shown in the figure, respectively. It is known that the tunnel of direct-gap requires degenerate state in the p-type and n-type material. The tunneling influence appears when the p-region carrier concentration is higher. The results are coincidence with theoretical analysis. Comparing the Fig. 3a with Fig. 3b, it is easy to be found that when $p > 10^{18}\ \mathrm{cm}^{-3}$, the tunnel of the triangular barrier hardly influences $(R_0A)_{\mathrm{total}}$, while the tunneling mechanism on the parabolic barrier type is the mainly source which reduces $(R_0A)_{\mathrm{total}}$ seriously, When $p < 10^{17}\ \mathrm{cm}^{-3}$, $(R_0A)_{\mathrm{total}}$ is determined by $(R_0A)_{\mathrm{GR}}$. In the range of $10^{17}\ \mathrm{cm}^{-3} < p < 10^{18}\ \mathrm{cm}^{-3}$, various R_0A components contribute to $(R_0A)_{\mathrm{total}}$. Fig. 4 shows that the dependence of $(R_0A)_{\mathrm{total}}$ and the R_0A components on the n-side carrier concentrate as a function of σN_{f} with the same parameters of Fig. 3 except for $p = 10^{17}\ \mathrm{cm}^{-3}$ instead of $n = 10^{18}\ \mathrm{cm}^{-3}$. Because of $(R_0A)_{\mathrm{GR}} \propto 1/(\sigma N_{\mathrm{f}})$, σN_{f} may be taken as one parameter. The tunneling mechanism may be neglected when p-region material has not degeneracy. From Fig. 4, we can see that R_0A is only limited by $(R_0A)_{\mathrm{GR}}$ in the condition of $\sigma N_{\mathrm{f}} \geqslant 0.01\ \mathrm{cm}^{-3}$. $(R_0A)_{\mathrm{GR}}$ increases with the increase of the carrier concentration of n-region or p-region. The reducing of σN_{f} obviously improves $(R_0A)_{\mathrm{GR}}$ and $(R_0A)_{\mathrm{total}}$, because of $D^* \propto \sqrt{R_0A}$, higher device performance can be obtained.

Observing Eqs. (10)–(12), the dependence of the quantum efficiency on some material parameters is found, such as carrier concentration, and surface recombination velocity, thickness, absorption coefficient and reflection coefficient. Moreover, the direction of the incident light also affects the quantum efficiency. Except illustrations in the following discussion, we choose $d = 5\ \mu\mathrm{m}$, $t = 5\ \mu\mathrm{m}$, $\mu_{\mathrm{h}} = 400\ \mathrm{cm}^2/\mathrm{V\ s}$, $\mu_{\mathrm{e}} = 3000\ \mathrm{cm}^2/\mathrm{V\ s}$, $S_{\mathrm{e}} = 0$; $S_p = 0$, $\sigma N_{\mathrm{f}} = 0.1\ \mathrm{cm}^{-1}$. In order to simplify the discussion, we consider the change of the quantum efficiency with two parameters, while other parameters keep constant and the direction of the incident light is from the n-side with the

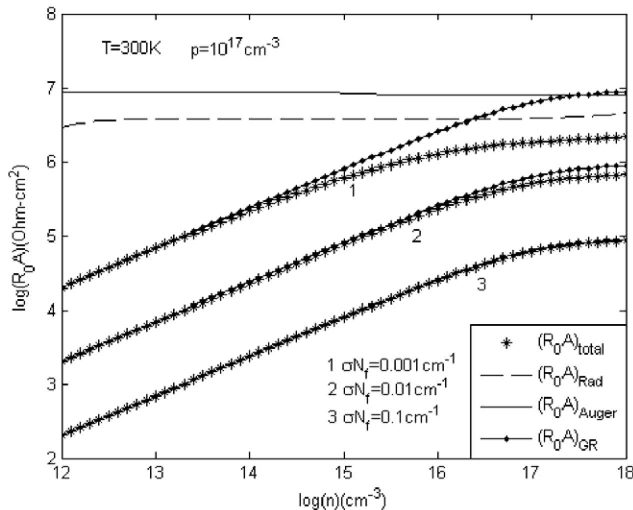

Fig. 4. The dependence of the R_0A components and total R_0A on n-side carrier concentration as a function of σN_{f}. In the condition of $d = 5\ \mu\mathrm{m}$, $t = 5\ \mu\mathrm{m}$, $\mu_{\mathrm{h}} = 400\ \mathrm{cm}^2/\mathrm{V\ s}$, $\mu_{\mathrm{e}} = 3000\ \mathrm{cm}^2/\mathrm{V\ s}$, $S_p = 0$, $S_{\mathrm{e}} = 0$.

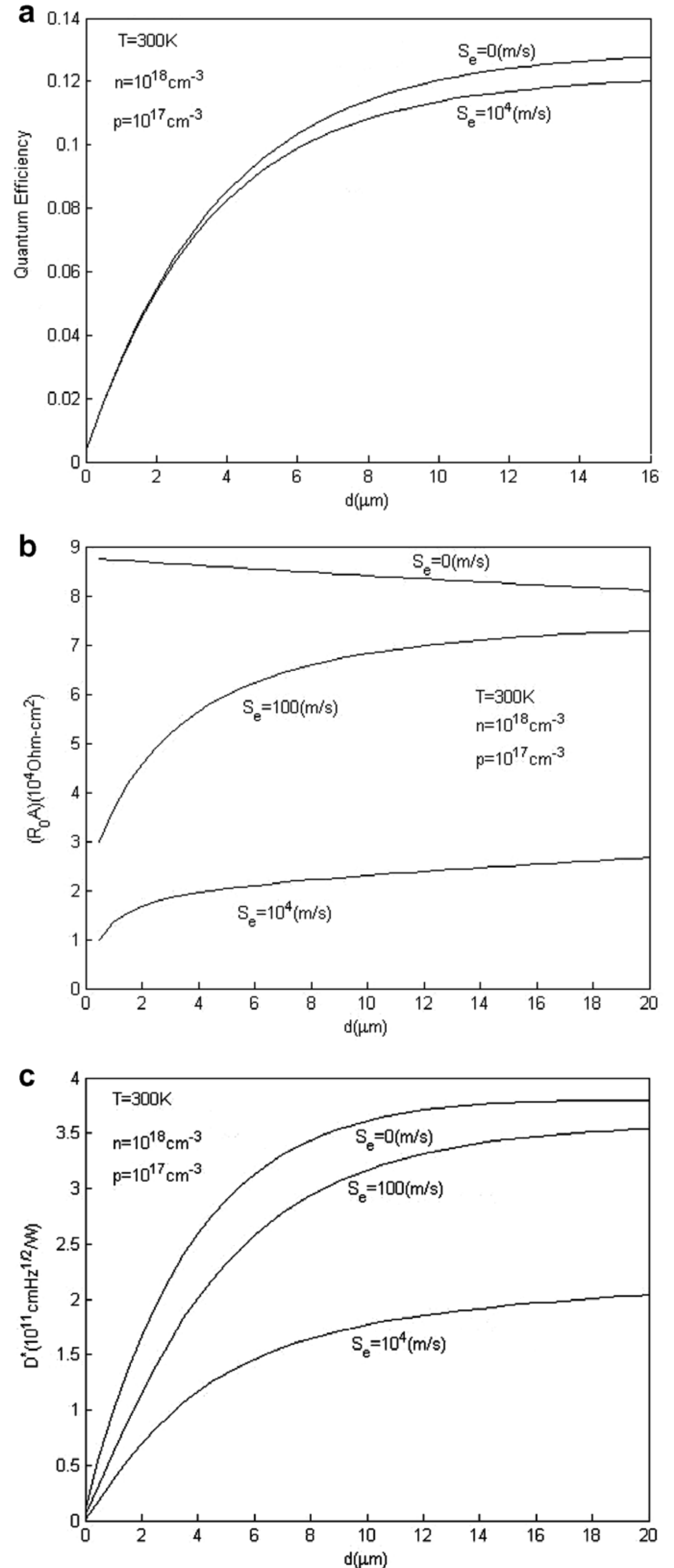

Fig. 5. The dependence of quantum efficiency, R_0A and detectivity on thickness and surface recombination velocity of the p-region with $t = 5\ \mu\mathrm{m}$, $\mu_{\mathrm{h}} = 400\ \mathrm{cm}^2/\mathrm{V\ s}$, $\mu_{\mathrm{e}} = 3000\ \mathrm{cm}^2/\mathrm{V\ s}$, $S_p = 0$, $\sigma N_{\mathrm{f}} = 0.1\ \mathrm{cm}^{-1}$.

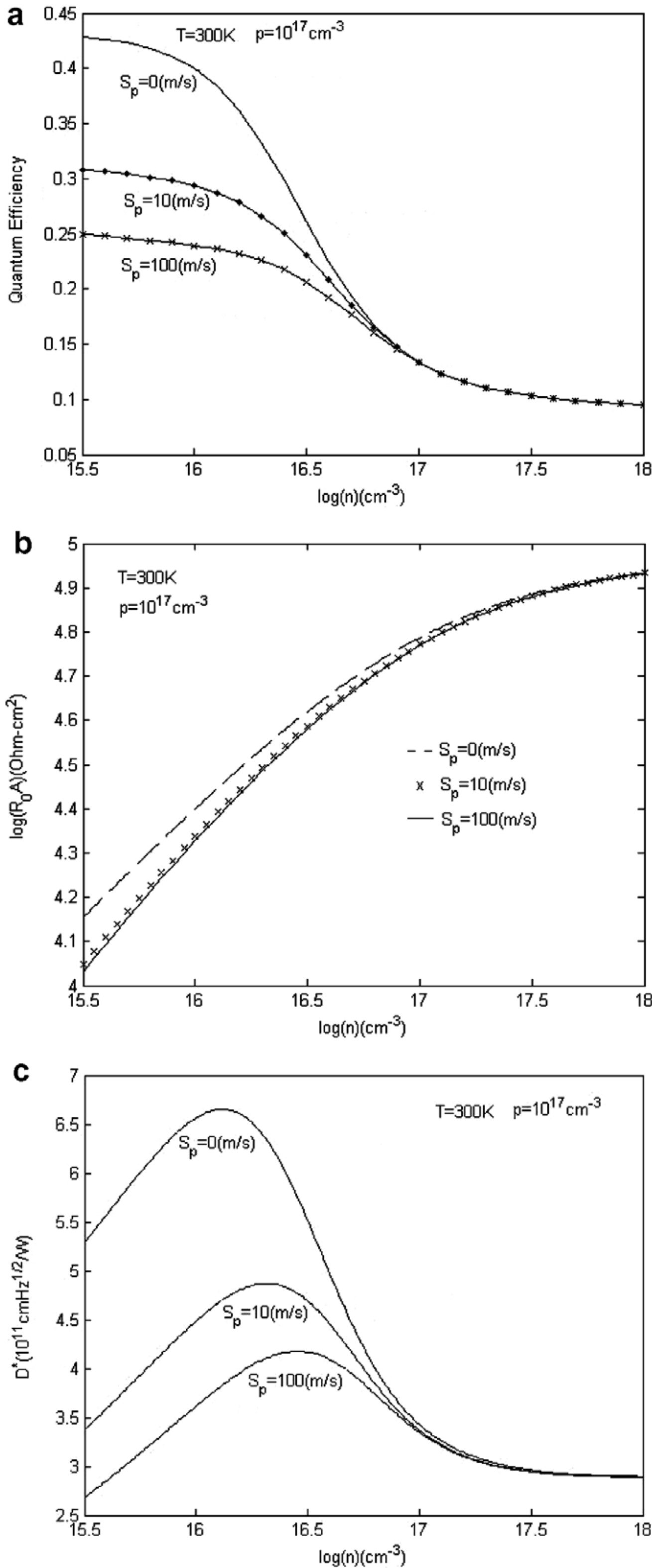

Fig. 6. The changes of the quantum efficiency, R_0A and detectivity versus n-side carrier concentration with surface recombination velocity S_p as a parameter. In the condition of $d = 5$ μm, $t = 5$ μm, $\mu_h = 400$ cm^2/V s, $\mu_e = 3000$ cm^2/V s, $S_e = 0$, $\sigma N_f = 0.1$ cm^{-1}.

wavelength 1.59 μm close to bandgap of $In_{0.53}Ga_{0.47}As$ material. Depending on the injected light energy, the

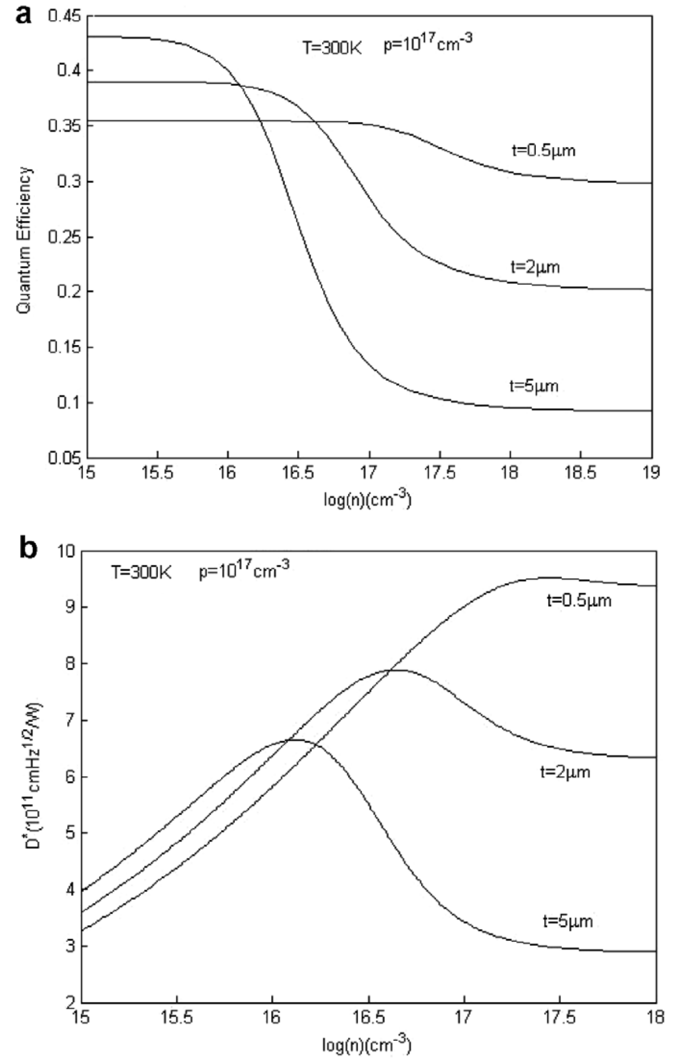

Fig. 7. A relationship of the quantum efficiency and detectivity with n-side carrier concentration for different n-side thickness. In the condition of $d = 5$ μm, $\mu_h = 400$ cm^2/V s, $\mu_e = 3000$ cm^2/V s, $S_p = 0$, $S_e = 0$, $\sigma N_f = 0.1$ cm^{-1}.

absorption coefficient is assumed to be $\alpha = 2.61 \times 10^5$ m^{-1} [12]. Fig. 5 shows the dependence of quantum efficiency, R_0A and detectivity on thickness and surface recombination velocity of the p-region with $n = 10^{18}$ cm^{-3}, $p = 10^{17}$ cm^{-3}. Due to light from the n side, the intensity is reduced through the n-region to lead to less the light absorption of p-region. Comparing Fig. 5a with Fig. 5c, we can find that surface recombination velocity of the p-region has little influence to the quantum efficiency. Because D^* is affected by the quantum efficiency and R_0A, it makes that surface recombination velocity has more influence to D^* than to quantum efficiency. Fig. 6a–c present the changes of the quantum efficiency, R_0A and detectivity versus n-side carrier concentration with surface recombination velocity S_p as a parameter, for $p = 10^{17}$ cm^{-3}. In Fig. 6a and c, it is implied that a influence of surface recombination velocity S_p to the quantum

efficiency and detectivity may be neglected when the *n*-side carrier concentration is more than $10^{17}\,\mathrm{cm}^{-3}$ and yet surface recombination velocity S_p has more effect to the quantum efficiency and detectivity when the *n*-side carrier concentration is less than $10^{17}\,\mathrm{cm}^{-3}$. D^* peak is appeared in Fig. 6c and position of peak moves towards low carrier concentration region when S_p reduces. Fig. 7 shows a relationship of the quantum efficiency and detectivity with *n*-side carrier concentration for different *n*-side thickness. An influence of *n*-side thickness to the quantum efficiency and detectivity is complex. From Fig. 7a and b, it is found that the increment with *n*-side thickness leads to reduce the quantum efficiency and detectivity within $n \geqslant 10^{17}\,\mathrm{cm}^{-3}$. This is because *n*-side thickness is increased to result in enhancing recombination probability. In Fig. 7b, D^* has peak value for the same thickness, and the position of peak moves with the change of *n*-side thickness. The thinner n-region contributes to elevate D^*. The result is basically in keeping with D^* reported by XeICs [13].

4. Conclusion

By the theory study on detectivity of $In_{0.53}Ga_{0.47}As$ photovoltaic detector, a result of the dependence the detectivity on material parameters has been obtained. Because D^* is determined by the quantum efficiency and R_0A, while the quantum efficiency and R_0A strongly depend on material parameters, it makes the dependence of D^* on carrier concentration, surface recombination velocity and thickness in the p-region and n-region. We have a conclusion that the influence of p-region material parameters and n-region material parameters on D^* is different when the incident light is from *n*-side. n-region material parameters may result in D^* change in the much extent. During the material growth and device fabrication, optimum material parameters will improve D^*. Our result is a using tool for fabricating higher performance InGaAs photovoltaic detector with lattice matched to the InP substrate.

Acknowledgements

This work was supported by China Postdoctoral Science Foundation No. 2004035568, Natural Science Foundation of China Contract No. 60676039 and 863 Project of China Contract No. 2202AA313080.

References

[1] Rogalski A. Infrared detectors: status and trends. Prog Quant Electron 2003;27:59–210.
[2] Olsen GH, Joshi AM, Mason SM, Woodruff KM, Mykietyn E, Ban VS, et al. Room-temperature InGaAs detector arrays for 2.5 μm. Proc SPIE 1989;1157:276–82.
[3] Olsen G, Joshi A, Lange M, Woodruff K, Mykietyn E, Gay D, et al. A 128 × 128 InGaAs detector array for 1.0–1.7 μm. Proc SPIE 1990;1341:432–7.
[4] Olsen GH. InGaAs fills the near-IR detector-array vacuum. Laser Focus World 1991:A21–30.
[5] Olsen GH, Joshi AM, Ban VS. Current status of InGaAs detector arrays for 1–3 μm. Proc SPIE 1991;1540:596–605.
[6] Joshi AM, Ban VS, Mason S, Lange MJ, Kosonocky WF. 512 and 1024 element linear InGaAs detector arrays for near-infrared (1–3 μm) environmental sensing. Proc SPIE 1992;1735:287–95.
[7] Cohen MJ, Olsen GH. Room temperature InGaAs camera for NIR imaging. Proc SPIE 1993;1946:436–43.
[8] Ettenberg MH, Lange MJ, O'Grady MT, Vermaak JS, Cohen MJ, Olsen GH. A room temperature 640 × 512 pixel near-infrared InGaAs focal plane array. Proc SPIE 2000;4028:201–7.
[9] Yuan T, Tianming Z, Baolin Z, Yixi J, Yongqiang N, Hong J, et al. Theoretical analysis of the Auger mechanism in a GaInAsSb infrared photovoltaic detector. Opt Eng 1998;37:1754–62.
[10] Yuan T, Tianming Z, Baolin Z, Yixi J, Hong J. Analysis of the R_0A product and detectivity in a GaInAsSb infrared photovoltaic detector. J Phys D: Appl Phys 1998;31:3291–7.
[11] Sze SM. Physics of semiconductor devices. 2nd ed. New York: Wiley; 1981. p. 513.
[12] Moss TS, Burrell GJ, Ellis B. Semiconductor opto-electronics. London: Chapel River Press; 1973. p. 48.
[13] XenIcs. 1.0–2.5 μm InGaAs Photodiode. May, 2003.